Provenance of quartz grains from soils over Quaternary terraces along the Guadalquivir River, Spain

A. Molinero-García [a], A. Müller [b,c], J.M. Martín-García [a,*], S.L. Simonsen [d], R. Delgado [a]

[a] *Departamento de Edafología y Química Agrícola (Facultad de Farmacia), Universidad de Granada, Spain*
[b] *Natural History Museum, University of Oslo, P.O. Box 1172 Blindern, 0318 Oslo, Norway*
[c] *Natural History Museum, Cromwell Road, London SW7 5BD, United Kingdom*
[d] *Department of Geosciences, University of Oslo, PO Box 1047 Blindern, N-0316 Oslo, Norway*

ARTICLE INFO

ABSTRACT

The characterisation of quartz grains' chemical and mineralogical properties in sediments and sedimentary rocks is widely used in provenance studies. This paper analyses quartz grains from the coarse sand fraction in soils in Quaternary fluvial terraces (Guadalquivir River, southern Spain). The tentative soil ages are 0.3 ka (Haplic Fluvisol), 7 ka (Haplic Calcisol), 70 ka (Cutanic Luvisol), 300 ka (Lixic Calcisol) and 600 ka (Cutanic Luvisol). The quartz grains analyses shed light on the sedimentological history of these terraces. Scanning electron microscope cathodoluminescence (SEM-CL) characteristics, micro inclusion inventory established by Energy-dispersive X-ray spectroscopy (SEM-EDX) and trace element contents determined with laser ablation inductively coupled plasma mass spectrometry (LA-ICP-MS) of quartz grains permitted distinguishing six types of grains in the soils studied: metamorphic quartz (type 1), undeformed granitic quartz (type 2), strongly altered granitic quartz (type 3), recrystallised (deformed) granitic quartz (type 4), sandstone-derived quartz (type 5) and hydrothermal quartz grains (type 6).

Metamorphic quartz grains (type 1) come from the Sierra Morena (Iberian Massif) and Sierra Nevada (Internal Betic Zone). Granitic quartz grains (types 2 to 4) come from Los Pedroches batholith and its associated plutons (Santa Elena and Linares). The sandstone-derived quartz type 5 comes from the numerous sandstone outcrops scattered in the central catchment area of the Guadalquivir River. Finally, hydrothermal quartz grains (type 6) originate from hydrothermal veins associated with subvolcanic rocks of the Los Pedroches batholith.

Variations were noted in the proportions of quartz types in soils of different ages, attributed to spatial and temporal changes in the catchment area. The most remarkable change occurred between 500 and 240 ka ago when the catchment area extended into Sierra Nevadás metamorphic rocks, well reflected in type 1 content (lower in P2, P4, P5 and PM) and their characteristics (quartz with less healed fractures, less Al content, bigger mica microinclusions, smaller Al/Ti ratio) in the post-500–240 ka soils.

Our study shows that the combined study of SEM-CL characteristics, micro inclusions (SEM-EDX), and trace element contents (LA-ICP-MS) of quartz grains is an efficient approach for characterising the provenance of quartz grains in the sand fraction of soils.

1. Introduction

Quartz is a major component of the soils (Drees et al., 1989) and is present in most sedimentary, metamorphic and igneous rocks. It is a tectosilicate with the formula SiO_2, in which silicon tetrahedrons share their oxygens in a three-dimensional structure, forming small channels that run parallel to the c axis (e.g. Rottier et al., 2017). In addition, its high hardness (7) and low solubility in water (11.0 ± 1.1 mg kg^{-1}, at 25 °C and 1 bar; Rimstidt, 1997) makes quartz a very stable mineral facilitating its enrichment in many sediments and clastic rocks (Blatt et al., 1980). In soils, it concentrates as pebble, sand and silt fractions (Calero et al., 2013; Martín-García et al., 2015).

Quartz is one of the chemically purest minerals in nature, after diamond and graphite (Drees et al., 1989). It contains, however, lattice-bound trace elements in low concentrations due to atomic substitution of Si and interstitial elemental incorporation within the crystal

structure. In addition, quartz may contain micro inclusions of solid, liquid or gaseous phases.

Al, Ti, Li, Ge, H, Be, B, Mn, Rb, Sr, Na, P, K, Ca, and Fe are the most common trace elements in natural quartz (e.g. Bambauer, 1961; Kats, 1962; Weil 1984, 1993; Perny et al., 1992; Larsen et al., 2000; Götze et al., 2004; Müller and Koch-Müller, 2009). Concentrations of these elements are directly determined with *in situ* micro-beam techniques, such as electron probe micro analysis (EPMA), laser ablation inductively coupled plasma mass spectrometry (LA-ICP-MS) and secondary ion mass spectrometry (SIMS) (e.g. Müller et al., 2003) or with spectrometric methods, such as FTIR spectrometry (e.g. Stalder et al., 2017). Cathodoluminescence (CL) is an imaging and spectroscopic technique, which reveals the relative abundance and distribution of lattice defects and impurity trace elements within quartz grains. As such, CL visualises structures related to crystallisation, such as growth zoning and secondary processes (alteration, recrystallisation or radiation damage) (Ramseyer and Mullis, 1990; Götze et al., 2001; Richter et al., 2003; Götze, 2012; Sales de Oliveira et al., 2017).

Physicochemical conditions strongly control the incorporation of trace elements in quartz and the formation of lattice defects during its crystallisation (e.g. Götze, 2009 and references therein). Thus, the trace element and lattice defect diversity and abundance detected along with the micro inclusion inventory are genetic fingerprints. The combination of quartz CL imaging and spectrometry with results of *in situ* micro-beam techniques (EPMA, LA-ICP-MS, SIMS) permits reconstructing the crystallisation and alteration processes using compositional and defect variations to estimate formation pressure, temperature and fluid or melt composition. Because quartz is relatively resistant to alteration and weathering compared to other minerals, it is increasingly used in provenance surface environment studies (Müller and Knies, 2013; Ackerson et al., 2015; Sales de Oliveira et al., 2017). However, there are no studies that apply these techniques to quartz grains in soils.

There are a few microchemical studies of quartz from granulometric fractions of soil. For example, Martín-García et al. (2004, 2015) obtained evidence of quartz alteration in the fine sand fraction (50–250 μm) of soils, developed on mica schist formations in Sierra Nevada, southern Spain, by scanning electron microscope backscattered electron (SEM-BSE) imaging, EPMA, high-resolution transmission electron microscopy (HRTEM) and selected area electron diffraction (SAED). They detected an increase of the trace element content on the edges of quartz grains in the Parent Rock < Entisol < Inceptisol < Alfisol evolution sequence.

This paper studies the quartz grains of the sand fraction from Quaternary soils forming terraces along the Guadalquivir River. The tentative ages of the terraces range between 0.3 and 600 ka (Calero et al., 2008). The bedrocks exposed in the river catchment area have a wide lithological variety (igneous, metamorphic and sedimentary rocks) belonging to the Iberian Massif, Internal Betic Zone and External Betic Zone. The sand fraction of these soils, which has been studied before by Martín-García et al. (2020), consists of a great mineral variety, including mainly quartz, K-feldspar, plagioclases, muscovite, illite, biotite, paragonite, chlorite, mixed-layered clay minerals, goethite, hematite, calcite and dolomite. These authors suggested the provenance of some of these minerals: 1) garnet (pyralspite group) and andalusite originate from metamorphic rocks of the Iberian Massif or the Internal Betic Zone; 2) andradite (garnet) is a typical constitute of calcareous, contact metamorphic rocks, found close to the Los Pedroches batholith (Iberian Massif – External Betic Zone contact); 3) staurolite, as a medium- to high-grade metasedimentary mineral (regional metamorphism), possibly comes from metapelites of the Internal Zone of the Betic Cordilleras; and 4) rutile, which is ubiquitous, was evidently neoformed in these soils, invalidating the possibility of using it as a mineral index in the provenance studies.

The great abundance of quartz grains in the sand fraction of the soil chronosequence from the Guadalquivir River (Calero et al., 2009; Martín-García et al., 2020) makes it an ideal provenance pathfinder. Therefore, the main objective is to determine the provenance of the

quartz grains that constitute the soils of the Guadalquivir River's chronosequence between 0.3 and 600 ka. To do so, we combined SEM-CL and LA-ICP-MS on quartz grains of the sand fraction (500–2000 μm). This is the first time this method combination is applied to quartz grains in soils. Finally, the results are compared and discussed regarding the provenance of other mineral soil grain suggested by Martín-García et al. (2020).

2. Geological setting and sample origin

The study area is located in the Cenozoic Guadalquivir Basin, drained by the Guadalquivir River, the largest river system in the southern Iberian Peninsula. Along the Guadalquivir River shores, a complex fluvial terrace system has developed during Quaternary. Soil sampling has been carried out on terraces of different ages located between the cities of Andújar and Villanueva de la Reina, along a 3.7 km long transect of the river between 3° 50′ – 4° 3′ W and 38° 0′ – 38° 2′ N (Fig. 1c).

The Cenozoic Guadalquivir Basin developed between the Iberian Massif to the north and the Betic Cordilleras to the south (Fig. 1a). The Quaternary fluvial alluvium of the Guadalquivir Basin consists of gravels with some stone-free sandy, silty layers originating from remarkably diverse lithology (Fig. 1). According to Martín-García et al. (2020), these rocks comprise: igneous rocks (granite, granodiorite, rhyolite, tonalite, andesite, and gabbro) and metamorphic rocks (schists, quartzites) from the Iberian Massif; sedimentary rocks (clays, sands, gravels, breccias, sandstones, limestones, marly limestones, marls and dolostones) from the External Betic Zone of the Betic Cordilleras; and sedimentary (limestones and dolostones) and metasedimentary rocks (schist, quartzites, shales, phyllites, marble and gneiss) from the Internal Betic Zone of the Betic Cordilleras.

The mineralogical diversity observed in the fluvial alluvium is related to the complex history of the catchment area of the Guadalquivir River, which has changed over time (Fig. 1b). The catchment of the sampling area is currently 17700 km^2, but 500–240 ka ago, it was much smaller (approx. 10420 km^2). Until then, there was an endorheic lake, the Guadix-Baza basin, into which the Guadiana Menor river drained (Demuro et al., 2015; García-Tortosa et al., 2019). Guadiana Menor river is a side stream of the Guadalquivir River in the eastern part of its current catchment area. Between 500 and 240 ka ago, due to Alpine tectonics and erosion, the Guadix-Baza basin drainage was strongly modified, and the endorheic lake became an exorheic lake, which started to drain towards the Atlantic Ocean via the Guadalquivir River (Ortiz et al., 2000). As a result, the catchment area became as twice as large, and for the first time, material from the Internal Betic Zone contributed to the formation of the terraces and floodplain of the Guadalquivir River in the study zone.

The soils studied in this paper developed on the surfaces of four Quaternary terraces and the floodplains (Table 1). These sequences have the following tentatives ages (Calero et al., 2008): 600 ka (P1; Terrace 1), 300 ka (P2; Terrace 2), 70 ka (P3; Terrace 3), 7 ka (P4; Terrace 4) and 0.3 ka (P5; floodplain). Samples were taken from all five environments. In addition, fresh point bar sediments (PM) were collected in the Guadalquivir River from an active bar of streams. Soil typologies are as follows (IUSS Working Group WRB, 2015): P1, Cutanic Luvisol; P2, Lixic Calcisol; P3, Cutanic Luvisol; P4, Haplic Calcisol; P5, Haplic Fluvisol.

The transformation of the ancient endorheic lake of the Guadix-Baza basin into an exorheic lake and the related catchment extension of the Guadalquivir River between 500 and 240 ka ago caused the sediments from the Internal Betic Zone rocks to become part of the material deposited on terraces (2, depending on the age of the catchment extension), 3 and 4 (affecting profiles (P2), P3, and P4), on the floodplain (profile P5) and the current riverbed point bar (PM).

The climate is currently hot Mediterranean with 500 mm total annual rainfall and a mean annual temperature of 18 °C. The vegetation is mainly anthropogenic because the flat surfaces are used, from time immemorial, as farmland (nowadays, olive groves, wheat and cotton).
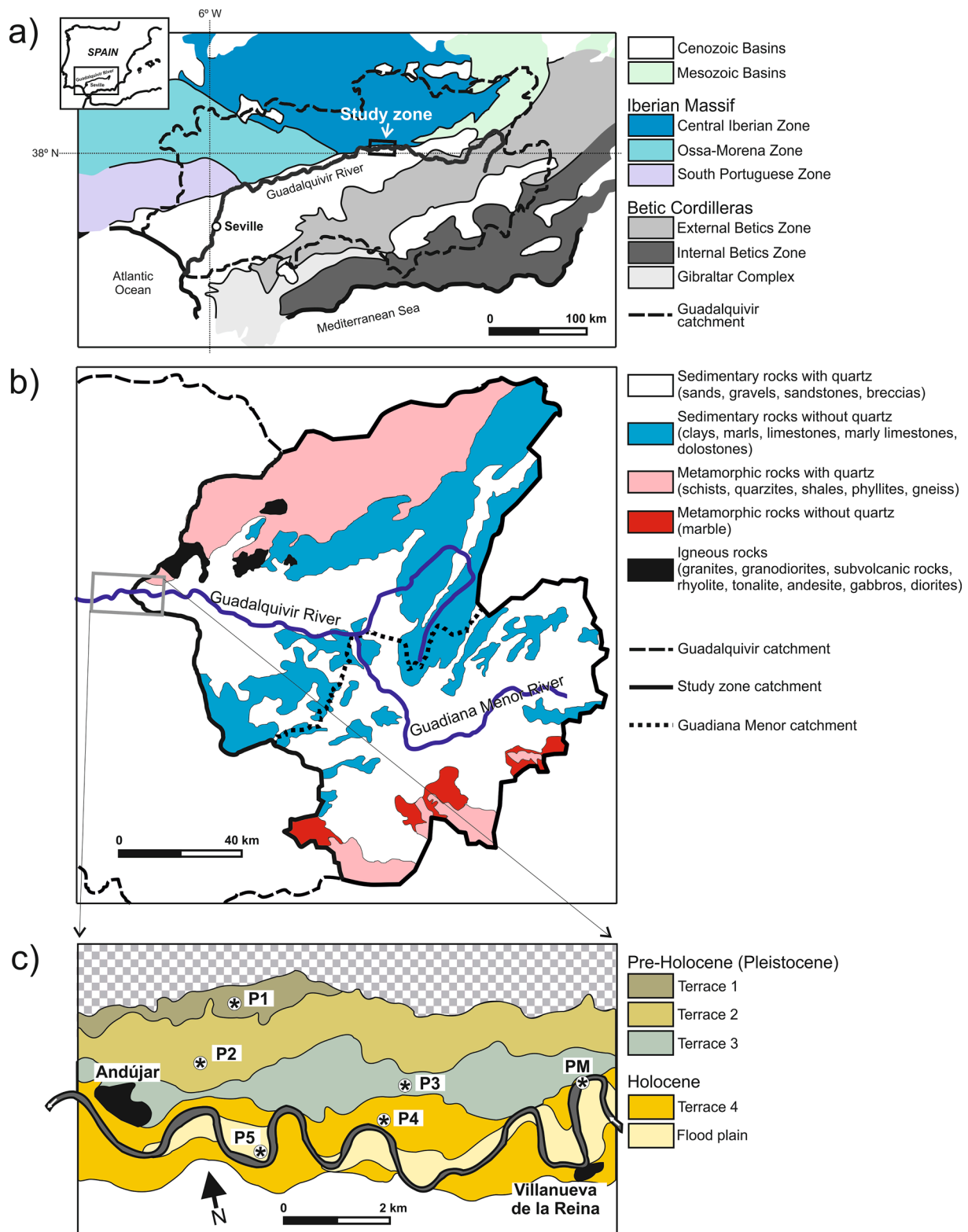
Fig. 1. Geology of the study area. a) Location of the study area in relation to the Iberian Massif and Betic Cordilleras; b) Simplified lithology of the Guadalquivir river catchment area; c) Detailed map of the sampling area with indicated positions of fluvial terraces and soil sampling sites.

The solum of the older terraces (pre-Holocene soils: P1, P2, and P3) shows Bt horizons (with clay illuviation features such as clay cutans), red munsell colours, relatively deep thickness, clayey texture (>30% clay) and evidence of carbonates leaching (and accumulation, in P2). Thus, the older soils have the greatest Harden's Profile Development Indexes (between 44.8 of P1 and 39.6 of P3; Table 1). In the Holocene

soil P4, brunification (Fe oxide precipitation) and some leaching/accumulation of carbonates has also been detected. P5 have no pedogenic evolution features.

The processes of weathering, leaching and carbonate accumulation, clay illuviation, reddening and soil structuration have affected the morphological, analytical and mineralogical properties of these soils

Table 1

Main characteristics of investigated soil samples according to Calero et al. (2008, 2009, 2013) and Martín-García et al. (2016).

Chronosequence level (soil profile)	P1	P2	P3	P4	P5	PM
Age (ka)	600, pre-Holocene	300, pre-Holocene	70, pre-Holocene	7, Holocene	0.3, Holocene	0.001, Holocene
Soil classification[a]	Cutanic Luvisol/ Palexeralf	Lixic Calcisol/ Haploxeralf	Cutanic Luvisol/ Haploxeralf	Haplic Calcisol/ Calcixerept	Haplic Fluvisol/ Xerofluvent	Alluvial[b]
PDI	44.8	44.3	39.6	26.8	21.2	0
Horizons sequence	Ap, Bt, Btg1, Btg2, 2BCtg, 3BCt, 4C	Ap, Btg1, Btg2, Btk, Cmk/Btk	Ap1, Ap2, Bt1, Bt2, Bt3, Bt4, Bt5, 2Bt6, 3Bt7	Ap1, Ap2, Bwk1, 2Bwk2, 3C1, 4C2	Ap, 2C1, 3C2, 4C3, 5C4, 6C5, 7C6	Point-bar deposit
Horizonte selected (sample name)	Btg2 (QAG04)	Btg2 (QAG10)	Bt4 (QAG18)	Bwk1 (QAG24)	Ap (QAG29)	(QAG38)
Moist colour (Munsell)	5YR 4/6	7.5YR 4/6	5YR 4/4	10YR 5/4	10YR 4/3	2.5Y 5/3
Clay (%)	27.4	41.7	42.0	30.1	23.0	16.3
Coarse sand (0.5–2 mm) (%)	26.5	1.9	18.8	22.8	3.5	45.3
Organic carbon (%)	0.15	0.40	0.27	0.30	0.77	1.76
Carbonates (%)	0.0	4.4	0.0	36.0	38.4	23.5
pH	7.2	7.8	7.4	8.1	7.9	8.4
CEC (cmol$_+$kg^{-1})	6.9	14.7	29.1	12.2	12.8	8.7

Abbreviations: PM - Parent material (current river sediments); PDI - Profile Development Index (according to Harden, 1982); CEC - Cation Exchange Capacity.

[a] Word Reference Base for Soil Resources/Soil Taxonomy.

[b] Recent sediments.

which vary over time, establishing an ideal chronosequence (Calero et al., 2008, 2009) also evidenced in the clay fraction formed (Calero et al., 2013; Martín-García et al., 2016) and fine sand fraction of these soils (Martín-García et al., 2020).

3. Material and methods

3.1. Sample preparation

Coarse sand grains (500–2000 µm) of five soil samples (one horizon per terrace was selected, choosing the one of greatest pedogenic evolution; Martín-García et al., 2020) and the point bar sediment of the Guadalquivir riverbed were separated (Table 1). First, the bulk soil samples and sediment PM were air-dried and sieved to <2 mm to obtain the fine earth fraction (<2 mm). Then and after removing organic matter with H$_2$O$_2$, the coarse sand fraction (500–2000 µm) was separated by wet sieving and collected on quartered aliquots to extract the quartz grains. A total of 1011 grains (between 131 and 217 grains in each sample) (Table 2) were hand-picked from the coarse sand fraction. Finally, the grains were embedded in epoxy resin on petrological standard glass slides (4.8 × 2.8 × 0.5 mm) and polished down half grain size for SEM, SEM-CL and LA-ICP-MS analysis.

3.2. Analytical methods

All 1011 quartz grains were first examined at the SEM, a Hitachi S–3600 N equipped with an energy-dispersive X-ray spectroscopy detector (EDX) from Bruker XFlash® 5030. The instrument is based at the Natural History Museum of Oslo. BSE imaging was used to map the grains, and EDX was applied to identify micro inclusions in quartz. BSE-SEM imaging and EDX semi-qualitative analyses of micro inclusions

were performed on 160 representative quartz grains, in which 275 micro inclusions were identified with EDX.

A total of 297 grains out of 1011 were randomly selected (sample by sample) for SEM-CL study (Table 2). At least 20 grains were studied (in each sample) in order to obtain a number of grains statistically representative (Mahaney, 2002). The CL images were acquired with a Delmic Sparc Advanced CL System attached to a Hitachi SU5000 FE-SEM based at the University of Oslo. The instrument settings of SEM-CL imaging were a dwell time of 50 µs and a gain of 650 mV. The settings for CL spectrum acquisition were a voltage of 12 kV, an exposure time of 200 ms and a beam input slit of 500 µm. This way, grain-specific, intra-granular features such as growth zoning or alteration patterns were mapped, and CL spectra were recorded to identify the wavelengths of emission bands causing the different CL colours of the examined quartz grains. The criteria established by Müller (2000), Götze et al. (2001), Bernet and Bassett (2005), Müller et al. (2010) and Sales de Oliveira et al. (2017) were used for identifying the quartz origin. This approach utilizes CL-SEM features of quartz grains and quartz CL emission characteristics, which provide information about the type and distribution of lattice defects, which in turn reflect the physico-chemical conditions of crystal growth.

From the 297 grains, 51 grains were selected for LA-ICP-MS analysis. In addition to SEM-BSE and SEM-CL observations, the selection was based on examination at the petrological microscope. Only grains without visible micro inclusions were chosen. The ICP-MS used in this study was a double-focusing sector field instrument of the ELEMENT-1 Finnigan MAT type combined with a New Wave UP-193 nm excimer laser probe. Continuous raster ablation was carried out, resulting in ablated rasters of approximately 150 × 100 µm with depths of 20 to 30 µm. Element concentrations were calculated by multi-standard calibration. The analysed elements and their detection limits (in ppm, in

Table 2

Frequency (and percentage) of quartz grains from coarse sand by quartz types.

Profile	Soil Horizon	Total grains	Quartz type[a] (percentage in parenthesis)					
			Type 1	Type 2	Type 3	Type 4	Type 5	Type 6
P1	Btg2	38	23 (60)	4 (11)	6 (16)	3 (8)	0 (0)	2 (5)
P2	Btg2	47	9 (19)	18 (38)	4 (9)	1 (2)	15 (32)	0 (0)
P3	Bt4	55	0 (0)	52 (94)	1 (2)	2 (4)	0 (0)	0 (0)
P4	Bwk1	60	17 (28)	34 (57)	3 (5)	4 (7)	2 (3)	0 (0)
P5	Ap	53	14 (26)	26 (49)	4 (8)	7 (13)	2 (4)	0 (0)
PM		44	4 (9)	26 (60)	1 (2)	11 (25)	1 (2)	1 (2)
TOTAL		297	67 (23)	160 (54)	19 (6)	28 (9)	20 (7)	3 (1)

[a] Type 1: metamorphic quartz; Type 2: undeformed plutonic quartz; Type 3: strongly altered plutonic quartz; Type 4: recrystallised plutonic quartz originating from metamorphic rocks; Type 5: sandstone quartz; Type 6: hydrothermal quartz

parentheses) were Al (9.46), Li (0.41), Be (0.08), B (1.29), Mn (0.07), Ge (0.10), Rb (0.09), Sr (0.01), Sb (0.01), U (0.01), Na (46.6), P (1.60), K (8.16), Ca (21.60), Ti (0.75), Fe (1.29), Zn (1.42) and Ga (0.06). The isotope ^{29}Si was used as the internal standard applying the stoichiometric concentration of Si in SiO_2. External multistandard calibration was performed using three silicate glass reference materials produced by the National Institute of Standards and Technology, USA (NIST SRM 610, 612, and 614). In addition, the applied standards included the NIST SRM 1830 soda-lime float glass (0.1% m/m Al_2O_3), the certified reference material BAM No. 1 amorphous SiO_2 glass from the Federal Institute for Material Research and Testing in Germany, and the Qz-Tu synthetic pure quartz monocrystal provided by Andreas Kronz from the Geowissenschaftliches Zentrum Göttingen (GZG), Germany. Certified, recommended, and proposed values for these reference materials were taken from Jochum et al. (2011) and from the certificates of analysis where available. For the calculation of P concentrations, the procedure of Müller et al. (2008) was applied. An Ar blank was run before each reference material and sample measurement to determine the

background signal. The background was subtracted from the instrumental response of the reference material/sample before normalization against the internal standard in order to avoid effects of instrumental drift. This was carried out to avoid memory effects between samples. A weighted least squares regression model, including several measurements of the six reference materials, was used to define the calibration curve for each element. Ten sequential measurements on the BAM No.1 SiO_2 quartz glass were used to estimate the limits of detection (LOD) which were based on $3 \times$ standard deviation (3σ) of the 10 measurements. Occasionally individual solid or fluid inclusions were hit by the laser. These analyses were recognisable from concentration spikes in the time-resolved analytical spectra; these data were not considered.

4. Results

Based on SEM-BSE and SEM-CL imaging, six types of quartz grains are distinguished. In addition, the trace elements contents, determined by LA-ICP-MS, are considered in the discrimination of quartz grain
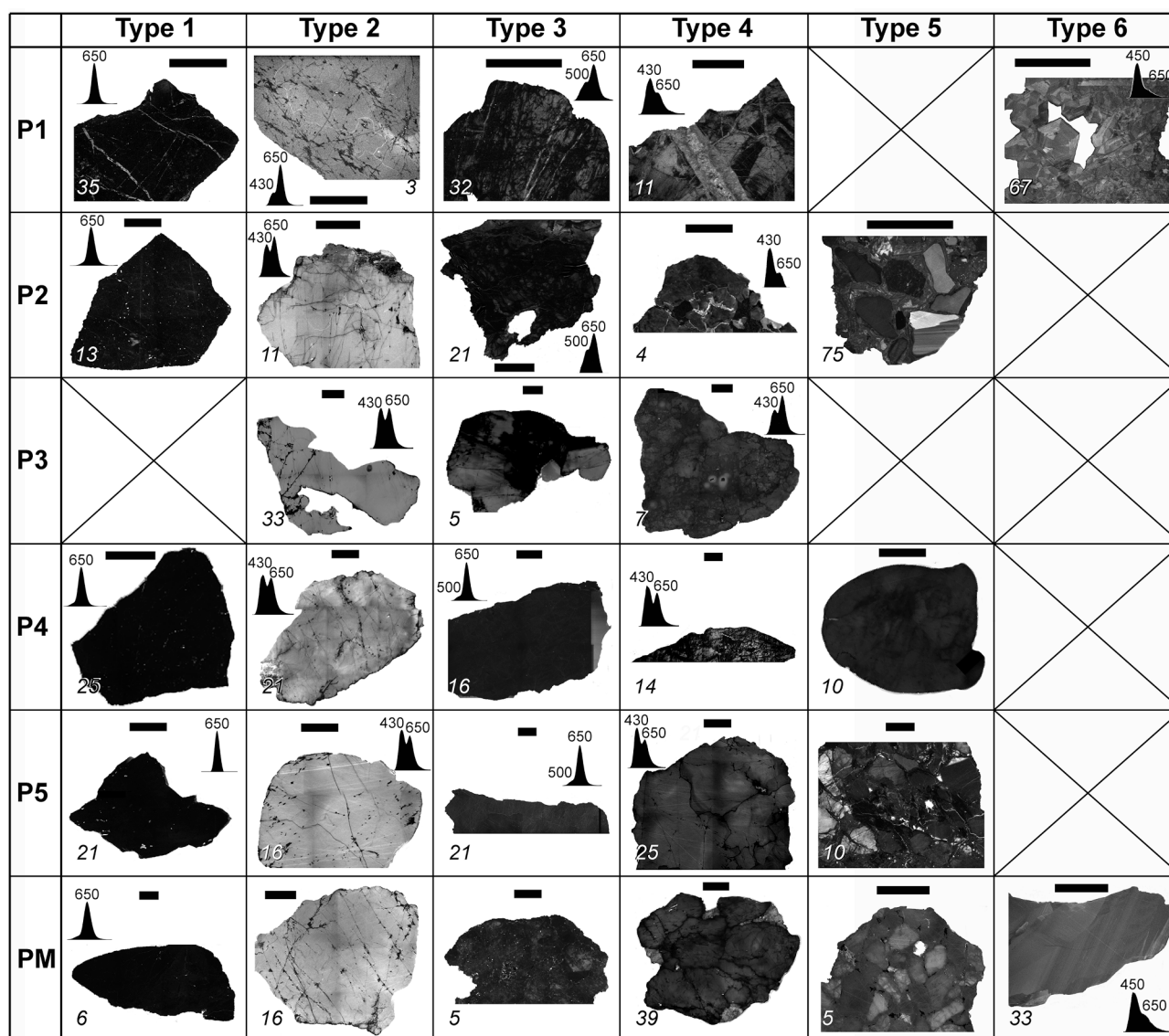
Fig. 2. Classification of quartz grains of soil sand fraction (>500 μm) based on CL characteristics. One representative SEM-CL image of each quartz grain type in each sample is shown. The number in the lower left of the cells indicate the grain abundance (in percent) in respect to the total number of identified grains of this type. The scale bar length correspond to 200 μm. Representative CL spectra with indicated peak maximum wavelength numbers (in nm) are provided for grains. Type 1: Metamorphic quartz grains; Type 2: Undeformed quartz grains originating from plutonic rocks; Type 3: Strongly altered plutonic quartz grains; Type 4: Recrystallised quartz grains from deformed plutonic rocks; Type 5: Sandstone quartz grains; Type 6: Hydrothermal quartz grains.

types.

4.1. Grain type 1: Metamorphic quartz

The type 1 population, comprising 67 (23%) out of 297 grains, is characterised by a monocrystalline structure and subangular-rounded grain shape (Table 2). The grains show one characteristic red emission band at ~650 nm in CL spectra (Fig. 2) and a homogeneous dull red-brown CL (Fig. 3). The spectra are uncommon because natural quartz usually has two broad emission bands, besides the red one also a blue band at ~450 nm (e.g. Götze et al., 2001). Type 1 is present in all profiles except P3. The P1 sample had the highest frequency of type 1, more than half of the grains studied (Table 2). Only a few mineral inclusions with little variety were detected (Table 3): mica, feldspar, zircon and rutile. The abundance and type of these micro inclusions is a specific feature of grain type 1.

In SEM-CL, some type 1 grains are cross-cut by thin, healed, brightly luminescent fractures and mostly with preferred orientation (Fig. 3a and b) and others type 1 grains do not show fractures (Fig. 3c). The CL spectrum of quartz healing these fractures exhibits both emission bands whereby the blue band dominates over the red one. The number of grains exhibiting these fractures varies in each sample depending on whether the soil is pre-Holocene or Holocene: in P1 and P2 (pre-Holocene), these fractures appear in most grains (68 and 56%, respectively), whereas in P4, P5 and PM (Holocene) grains, these fractures are scarce or absent (24, 0 and 0%, respectively).

The metamorphic origin of these quartz grains is suggested because of their weak reddish-brown CL, the absence of growth zoning and healed fluid pathways (typical of igneous quartz) and deformation lamellae characteristic of high-grade metamorphic quartz (Müller,
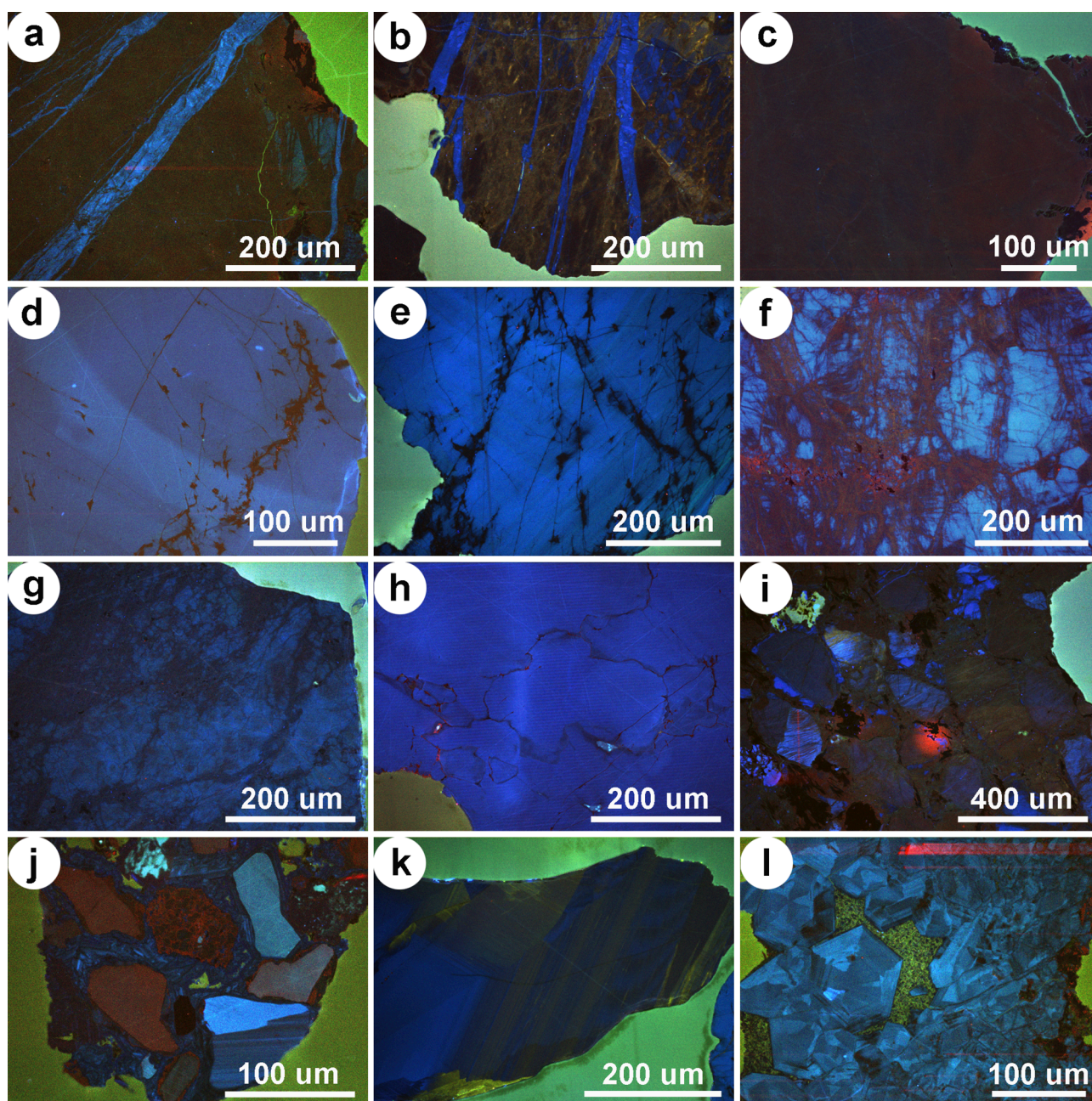

Fig. 3. SEM-CL color images of quartz sand grains. a) type 1 (from P1); b) type 1 (P4); c) type 1 without fractures (P2); d) type 2 (P1); e) type 2 (PM); f) type 3 (P2); g) type 4 (P5); h) type 4 (PM); i) type 5 (P5); j) type 5 (P2); k) type 6 (PM); l) type 6 (P1).

Table 3
Mineral micro inclusions identified in the studied quartz grains.

	P1 (N = 37)		P2 (N = 25)		P3 (N = 22)		P4 (N = 23)		P5 (N = 22)		PM (N = 31)		TOTAL (N = 160)		
	n	mean size (µm)	n	mean size (µm)	n	mean size (µm)	n	mean size (µm)	n	mean size (µm)	n	mean size (µm)	n	mean size (µm)	%
Feldspar[a]	10	111 ± 87	11	209 ± 62	13	250 ± 225	5	254 ± 203	5	141 ± 77	13	268 ± 185	57	206	36
Muscovite[b]	18	29 ± 23	5	154 ± 129	5	103 ± 102	6	205 ± 199	5	137 ± 83	4	143 ± 43	43	128	27
Zircon	3	45 ± 13	2	38 ± 18	4	45 ± 37	2	18 ± 11	2	15 ± 14	5	52 ± 19	18	35	11
Iron Oxides[c]	5	46 ± 27	2	38 ± 18	2	13 ± 4	2	10 ± 0	1	20			14	25	9
Monazite	1	20			5	42 ± 36	3	42 ± 8	3	15 ± 9			12	30	8
Rutile	3	82 ± 59	4	58 ± 30					3	50 ± 36	1	45	11	59	7
Ilmenite	3	28 ± 19	4	34 ± 11			1	100	2	20 ± 21	1	100	11	56	7
Apatite	1	40	1	60	1	100	1	150					4	88	3
Gypsum									4	38 ± 15	1	50	5	44	3
Xenotime					2	45 ± 7	1	50					3	48	2
Cassiterite			1	90									1	90	1
Pyrite									1	5			1	5	1
Barite									2	45 ± 7			2	45	1
Antimony	1	5											1	5	1
TOTAL	45		30		32		21		28		25		183		

N = number of analysed quartz grains (among the grains that show micro inclusions); n = number of analysed micro inclusions by profile.

[a] The feldspar found was either K-feldspar or albite. Ca-bearing plagioclases (anorthite) has not been found.

[b] Muscovite and/or biotite.

[c] Goethite, hematite and/or magnetite.

2000; Bernet and Bassett, 2005; Sales de Oliveira et al., 2017).

The most abundant trace element is Al (192 ± 164 ppm), followed by Fe (95 ± 144 ppm) and K (61 ± 51 ppm). Mean element concentrations show high standard deviation values due to the variability among grains. Al/Ti values have a wide range and vary from 1.6 to 375.8. There are poor correlations between the contents of Al and K ($R^2 = 0.014$, n = 10) and Al and Li ($R^2 = 0.342$; n = 10) (Fig. SM1).

Type 1 grains differ from the other types described below. They have lower Ti than types 2, 4 and 5 (except for grains in sample P2), contain little Li compared to types 2 and 4 (except two cases) and in Holocene samples, are rich in Mn compared to the other types.

4.2. Quartz type 2: Undeformed plutonic quartz

Most of the grains studied (160 out of 297 = 54%) belong to type 2 (Table 2). This group comprises monocrystalline and subangular-angular quartz grains. Some grains are very angular. These grains have a relatively bright, violet to blue CL, and the CL spectra show two broad emission bands at ~430 and ~650 nm (Figs. 2 and 3). In most cases, the intensities of both emissions are similar. Occasionally, patches of dull CL and weakly contrasted growth zoning are developed (Fig. 3e). Randomly oriented fractures, which are healed with non-luminescent quartz, are common. These features are typical of plutonic quartz (Müller et al., 2010; Sales de Oliveira et al., 2017). Grains, which exhibit magmatic growth zoning (Fig. 3e), originate typically from subvolcanic or volcanic granitic rocks, such as rhyolites.

Type 2 is present in all samples in very variable abundance (Table 2, Fig. 2). Type 2 has the highest amount and variety of micro inclusions comprising mainly feldspar, mica, zircon and monazite. These are typical minerals of granitic rocks (Table 5).

The most abundant trace elements are Al, Ti and Li (>30 ppm usually) (Table 4). In type 2, no correlation has been detected between the Al and other elements.

Comparing the chondrite-normalised trace element values of type 2 and type 1 (Fig. 4), the following differences are noticed: Type 2 has more consistent compositions (closer lines), higher average concentrations of Li and Ti, and is depleted of Sb, Sr and Ge compared to type 1.

4.3. Quartz type 3: Strongly altered plutonic quartz

Type 3 represents a less abundant quartz population, comprising 19 (6%) out of 297 grains studied, although it is present in all samples

(Table 2). This type comprises monocrystalline and mainly subangular-angular to subangular-rounded grains with a patchy CL (Fig. 2 and Fig. 3f). The CL spectra show two emission bands at 500 and 650 nm, of which the 500 nm band is less pronounced. This grain population is interpreted as strongly altered plutonic quartz, which presumably originates from similar plutonic rocks as type 2, with the difference that the quartz was altered post-crystallisation by late magmatic or hydrothermal fluids.

Mineral inclusions are common and include rutile, mica, zircon, iron oxides and ilmenite (Table 5).

Two LA-ICP-MS analysis were performed only on this grain type. The grains are from samples P1 and P5. Both analyses differ considerably in their abundance of trace elements compared to other types (Table 4), with low Ti and exceptionally low Li.

4.4. Quartz type 4: Recrystallised (deformed) plutonic quartz

Type 4 quartz population comprises 28 (9%) out of 297 grains studied with SEM-CL. The group is characterised by polycrystalline clusters of recrystallised quartz grains, typical of quartz in deformed rocks. They have a heterogeneous morphology from subangular-angular to subangular-rounded grains. Frequently, they appear dark grey or black in panchromatic SEM-CL due to low CL intensities (Fig. 2). The CL spectra show two bands at 430 and 650 nm, similar to spectra of type 2 grains. Micro inclusions are common and comprise mainly mica and subordinate feldspar, zircon, iron oxides, monazite and gypsum (or anhydrite) (Table 5). Based on the observations, this population is interpreted as recrystallised (deformed) plutonic quartz. However, gypsum inclusions in some grains indicate that the originally plutonic quartz grains were deposited in sediments after their deformation before they ended up in the river terraces.

The highest number of type 4 grains was found in sample PM, followed by Holocene and pre-Holocene soil samples (Table 2).

Five microanalyses of this type (from P5 and PM) show that the most abundant elements are Al (289 ± 148 ppm), K (65 ± 52 ppm) and Ti (63 ± 21 ppm). Once again, the high standard deviation values reflect the variability among grains. Some samples have elevated values of Na, Fe, P, and Ca (Table 4). The Li content is lower than in type 2 but higher than in the other types. Al and K contents are very well correlated ($R^2 = 0.895$), which indicates that substitutional is charge-compensated partially by K^+ ($Si^{4+} \rightarrow Al^{3+} + K^+$; e.g. Müller and Koch-Müller 2009). Another noticeable correlation is detected in the Al and Ti relationship

Table 4

Mean values (and standard deviation) of trace elements contents (ppm) and Al/Ti ratio in quartz grains (LA-ICP-MS) from coarse sand.

	Profile	n	Al	Li	Be	B	Mn	Ge	Rb	Sr	Sb	U	Na	P	K	Ca	Ti	Fe	Zn	Ga	Al/Ti
	LOD		9.46	0.41	0.08	1.29	0.07	0.10	0.09	0.01	0.01	0.01	46.60	1.60	8.16	21.60	0.75	1.29	1.42	0.06	
type 1	P1	5	269.39 ± 143.17	8.39 ± 12.99	0.13 ± 0.06	3.55 ± 0.88	0.91 ± 0.51	1.62 ± 0.31	0.39 ± 0.27	1.21 ± 0.68	1.41 ± 0.82	<0.01	<46.6	2.09 ± 2.89	46.25 ± 28.19	<21.6	1.67 ± 0.46	37.25 ± 46.53	2.25 ± 1.41	0.13 ± 0.06	172.07 ± 120.74
	P2	1	393.68	34.05	0.20	5.33	1.21	1.05	0.39	0.12	1.17	<0.01	<46.6	3.86	92.08	<21.6	42.47	445.93	9.24	0.32	9.27
	P4	2	40.24 ± 41.08	1.62 ± 0.75	0.03 ± 0.02	2.08 ± 0.58	17.17 ± 18.01	1.36 ± 0.40	0.10 ± 0.09	3.10 ± 3.42	1.58 ± 0.25	0.03 ± 0.02	606.58 ± 824.88	8.79 ± 7.21	92.38 ± 125.61	214.85 ± 226.49	5.51 ± 1.92	24.42 ± 28.64	11.25 ± 5.98	0.43 ± 0.20	9.16 ± 10.65
	P5	2	49.19 ± 35.20	1.67 ± 0.85	0.09 ± 0.07	1.90 ± 0.34	25.24 ± 27.56	1.30 ± 0.38	0.52 ± 0.52	4.25 ± 0.91	1.13 ± 0.54	<0.01	155.53 ± 186.99	1.57	52.30 ± 16.55	86.15 ± 21.43	2.88 ± 0.02	134.70 ± 155.77	16.45 ± 15.06	0.11 ± 0.02	17.07 ± 12.11
Mean type 1		10	191.95 ± 164.11	8.26 ± 12.98	0.11 ± 0.07	3.10 ± 1.27	9.06 ± 15.39	1.45 ± 0.34	0.36 ± 0.29	2.09 ± 1.93	1.36 ± 0.60	0.01 ± 0.01	166.40 ± 369.08	3.50 ± 4.22	61.27 ± 51.00	69.12 ± 111.89	6.76 ± 12.66	95.04 ± 144.02	7.59 ± 8.16	0.21 ± 0.15	92.21 ± 116,63
type 2	P1	2	183.81 ± 47.30	21.21 ± 20.43	0.17 ± 0.13	3.98 ± 1.22	0.91 ± 0.62	0.94 ± 0.10	0.25 ± 0.27	0.57 ± 0.74	1.04 ± 1.39	<0.01	<46.6	<1.60	23.71 ± 24.49	<21.26	34.53 ± 23.08	14.01 ± 14.00	1.51 ± 1.12	0.12 ± 0.01	6.27 ± 2.82
	P2	6	228.97 ± 76.23	37.14 ± 20.14	0.18 ± 0.05	3.57 ± 1.19	1.07 ± 0.30	0.70 ± 0.06	0.17 ± 0.18	0.16 ± 0.17	1.41 ± 2.99	<0.01	<46.6	<1.60	41.43 ± 48.70	<21.6	54.86 ± 18.35	16.95 ± 9.79	2.95 ± 1.89	0.20 ± 0.14	4.44 ± 1.43
	P3	10	219.97 ± 82.09	38.05 ± 14.98	0.30 ± 0.36	2.22 ± 0.90	1.12 ± 1.44	0.90 ± 0.33	0.18 ± 0.20	0.06 ± 0.03	0.15 ± 0.17	<0.01	<46.6	8.33 ± 18.10	13.67 ± 13.19	29.03 ± 45.21	40.57 ± 14.95	14.68 ± 19.05	2.91 ± 1.34	0.18 ± 0.10	5.90 ± 2.56
	P4	5	310.63 ± 79.51	41.33 ± 18.03	0.27 ± 0.27	4.16 ± 3.18	1.82 ± 1.77	0.81 ± 0.20	0.37 ± 0.28	0.21 ± 0.16	0.22 ± 0.22	0.02 ± 0.02	54.56	8.94 ± 6.40	24.19 ± 8.71	40.02 ± 39.48	37.50 ± 15.80	9.25 ± 4.36	6.50 ± 4.06	0.31 ± 0.25	8.85 ± 2.25
	P5	3	223.86 ± 28.96	28.98 ± 16.42	0.17 ± 0.01	4.74 ± 2.84	1.43 ± 0.81	0.78 ± 0.08	0.66 ± 0.53	0.08 ± 0.07	0.22 ± 0.12	<0.01	188.89 ± 286.80	4.51 ± 3.26	97.07 ± 62.95	68.87 ± 27.21	79.08 ± 24.17	6.60 ± 4.60	3.75 ± 2.22	0.30 ± 0.09	3.04 ± 1.11
	PM	6	265.54 ± 54.65	51.50 ± 8.78	0.15 ± 0.18	3.63 ± 1.23	1.11 ± 0.57	0.75 ± 010	0.16 ± 0.07	0.09 ± 0.04	0.17 ± 0.14	<0.01	<46.6	3.11 ± 1.58	14.22 ± 13.13	24.77 ± 20.91	60.61 ± 21.54	27.79 ± 26.02	4.02 ± 1.48	0.25 ± 0.06	4.90 ± 2.02
Mean type 2		32	242.47 ± 74.99	39.01 ± 16.67	0.22 ± 0.24	3.39 ± 1.83	1.23 ± 1.10	0.81 ± 0.22	0.25 ± 0.27	0.14 ± 0.20	0.47 ± 1.34	<0.01	<46.6	5.28 ± 10.59	29.07 ± 36.71	29.62 ± 34.12	49.76 ± 21.41	15.91 ± 16.85	3.68 ± 2.42	0.22 ± 0.14	5.65 ± 2.58
type 3	P1	1	99.25	0.79	<0.08	6.36	2.28	1.50	0.40	0.12	1.03	<0.01	88.18	<1.60	29.97	<21.6	0.83	6.29	2.01	0.12	119.58
	P5	1	305.76	2.98	0.38	5.87	7.33	1.64	31.02	8.24	2.82	<0.01	156.71	<1.60	74.63	50.20	5.44	181.52	19.17	0.22	56.21
Mean type 3		2	202.51 ± 146.02	1.89 ± 1.55	0.21 ± 0.24	6.12 ± 0.35	4.81 ± 3.57	1.57 ± 0.10	15.71 ± 21.65	4.18 ± 5.74	1.92 ± 1.27	<0.01	122.44 ± 48.46	<1.60	52.30 ± 31.58	30.50 ± 27.86	3.13 ± 3.26	93.91 ± 123.91	10.59 ± 12.13	0.17 ± 0.07	87.90 ± 44.81
type 4	P5	1	161.67	16.73	0.45	2.76	0.15	0.26	0.61	<0.01	0.12	<0.01	334.34	36.29	48.54	156.28	44.20	1.63	16.30	1.62	3.66
	PM	4	320.37 ± 149.31	15.60 ± 10.98	0.19 ± 0.13	6.04 ± 4.76	1.31 ± 0.56	0.70 ± 0.12	0.23 ± 0.10	0.48 ± 0.43	0.28 ± 0.17	0.03 ± 0.03	<46.6	6.15 ± 2.38	68.95 ± 58.48	51.35 ± 54.35	67.72 ± 21.10	170.72 ± 248.44	3.97 ± 1.15	0.41 ± 0.30	4.65 ± 1.03
Mean type 4		5	288.63 ± 147.50	15.83 ± 9.52	0.24 ± 0.16	5.38 ± 4.37	1.07 ± 0.71	0.61 ± 0.22	0.30 ± 0.19	0.39 ± 0.43	0.24 ± 0.16	0.03 ± 0.03	<46.6	12.18 ± 13.64	64.87 ± 51.46	72.34 ± 66.47	63.02 ± 21.08	136.90 ± 228.06	6.43 ± 5.60	0.65 ± 0.60	5.65 ± 1.03
type 5	P4	1	196.74	0.37	4.27	3.85	1.28	0.52	<0.09	1614.84	<0.03	0.02	<46.6	5.95	20.61	<21.6	62.42	13.58	2.55	0.40	3.15
type 6	P1	1	837.98	2.22	0.09	5.76	0.28	2.10	0.59	1.08	0.58	<0.01	<46.6	1.61	208.73	39.3	1.97	43.39	2.39	0.16	425.37
Mean all types		51	236.20 ± 135.68	12.96 ± 20.88	0.28 ± 0.61	3.69 ± 2.15	3.33 ± 7.33	1.00 ± 0.42	0.89 ± 4.31	0.74 ± 1.58	0.67 ± 1.19	0.01 ± 0.01	74.15 ± 183.12	5.37 ± 9.70	48.30 ± 48.34	41.41 ± 60.88	36.93 ± 27.88	46.84 ± 101.86	4.94 ± 5.02	0.33 ± 025	33.91 ± 83.49

n – number of analyzed quartz grains. Mean values were calculated considering the mean value of the range for data above detection limit. LOD: Limit of detection.

Table 5
Frequency of micro inclusions in quartz grains sorted by quartz type.[a]

	Grouped profiles by age	n	Fd	m	Pb-m	Ru	Il	Sb	Zr	Fe-ox	Mo	Ca	Ap	Xe	Py	Gy
Type 1	Preholocenic (P1)	7	1[b]	4	4				1							
	Holocenic (P5)	2			1	1										
Type 2	Preholocenic (P2. P3)	13	6[c]	4	7				3	1	4	1	1	2		
	Holocenic (P4. P5. PM)	21	8[c]	7	14	1	2	1	6	1	3		1	1		
Type 3	Preholocenic (P1. P2)	4		1	2	3	1		1	1						
Type 4	Preholocenic (P1. P3)	3	1	3	3				1	1	1					
	Holocenic (P5. PM)	4	1[c]		2				1	2						1
Type 5	Preholocenic (P2)	4	2[c]			1	2		1	1						
	Holocenic (P5. PM)	2			1	1	1				1				1	
TOTAL		60	19	19	34	7	6	1	14	7	9	1	2	3	1	1

Abbreviations: n = number of analyzed quartz grains; Fd = feldspars; m = micas: biotite, muscovite or illite; Ru = rutile. Il = ilmenite; Sb = Sb-bearing mineral (unspecified); Zr = zircon; Fe-ox = iron(hydr)oxides: goethite, hematite or magnetite; Mo = monazite; Ca = Cassiterite; Ap = Apatite; Xe = xenotime; Py = pyrite; Gy = gypsum.

[a] Micro inclusion in type 6 grains have not been studied.
[b] K-feldspar.
[c] Albite and K-feldspar.
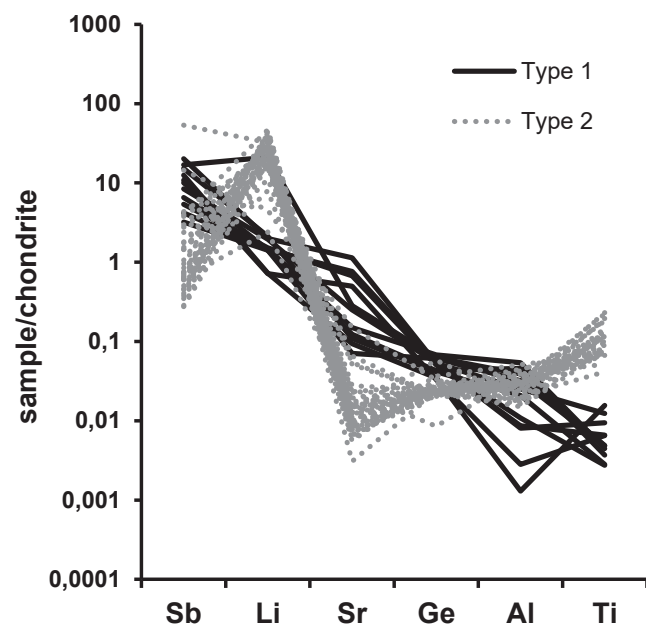
Fig. 4. Spider diagram depicting some trace element contents detected in type 1 and type 2 quartz grains normalized to carbonaceous chondrite (McDonough and Sun, 1995).

($R^2 = 0.817$).

4.5. Quartz type 5: Sandstone-derived quartz

Type 5 quartz grains comprise 20 (7%) out of 297 grains studied with CL (Table 2). Most type 5 grains (15) were identified in sample P2. Samples P1 and P3 do not contain this type. The grains are characterised either by clusters of well-rounded grains with variable CL cemented by non-luminescent authigenic quartz or by well-rounded single grains with remains of authigenic quartz overgrowths (Figs. 2 and 3). Based on these observations, type 5 grains originate from sandstone or arkose. However, the variable CL of the "primary", authigenic-quartz-embedded grains indicate different origins, such as metamorphic or plutonic rocks.

These grains show a diversity of mineral inclusions, including ilmenite, feldspar, zircon, rutile, monazite and pyrite (Table 5).

Microanalysis of type 5 (only of one grain from sample P4) show the following abundance: Al (197 ppm) > Ti (62 ppm) > K (21 ppm) (Table 4). The remaining elements have concentrations <20 ppm.

4.6. Quartz type 6: Hydrothermal quartz

The sixth grain type identified exhibits oscillatory growth zoning typical for hydrothermal quartz (Götze et al., 2001; Bernet and Bassett, 2005; Sales de Oliveira et al., 2017; Figs. 2 and 3). This quartz population is rare and comprised only 3 (1%) out of 297 grains (Table 2). The CL spectrum shows two emission bands, one high-intensity band at ~450 nm and a weak band at ~650 nm.

Due to their small grain size, trace element data were only acquired from one of the three grains. This grain has the highest Al of all quartz of 838 ppm studied, confirming the supposed hydrothermal origin of the grain (e.g. Rusk et al., 2008). The Al content is followed by K (209 ppm) > Fe (43 ppm) > Ca (39 ppm) (Table 3). Concentrations of the other elements are below 10 ppm. The high Ge content of 2.1 ppm is also characteristic of hydrothermal quartz (e.g. Götze et al., 2004).

5. Discussion

The provenance of the six types of quartz grains (previously defined and summarized in Table 6) and the approximate extension and change of the catchment area over time are discussed considering the following: 1) types of quartz, their relative abundance in the individual samples and change of the abundance over time; 2) micro inclusion inventory of quartz grains; 3) trace element content of the different quartz types, and 4) Ti content as an indicator of the quartz crystallisation temperature by applying the Ti-in-quartz geothermobarometer by Huang and Audétat (2012).

5.1. Quartz types and provenance

First, we checked if the corresponding rocks of the identified genetic quartz types (plutonic, metamorphic, sedimentary and subvolcanic rocks) occur in the current and historic river catchment areas (Fig. 1).

In today's catchment area, several plutons (Santa Elena and Linares) belonging to the Los Pedroches batholith are exposed (Fig. 1b). Although the pluton exposures are relatively small compared to other rock types, they are close to the sampling area and, thus, most likely the protoliths of the most common quartz type of our study, type 2 and of the other plutonic quartz types 3 and 4. All three types appear in all samples studied.

Besides plutonic rocks, there are abundant metamorphic rocks in the catchment area, both in Sierra Morena (Iberian Massif) to the north and Sierra Nevada (Internal Betic Zone) to the south (Fig. 1b). These rocks are most likely the source of our metamorphic quartz type 1. It is the second most common quartz type in our samples. Based on SEM-CL characteristics, type 1 grains are subdivided into two groups: grains of the pre-Holocene samples (P1 and P2) commonly exhibit quartz-healed,

Table 6
Features of quartz grains types from the study area.

	Type 1	Type 2	Type 3	Type 4	Type 5	Type 6
Structure and morphology	monocrystalline and subangular-rounded	monocrystalline and subangular-angular (even very angular)	monocrystalline and subangular-angular to subangular-rounded	polycrystalline cluster of recrystallised quartz and subangular-angular to subangular-rounded	cluster of grains or well-rounded single grain	not applicable
CL appearance	homogeneous dull red-brown	bright, violet to blue	patchy	dark grey or black (panchromatic SEM-CL)	variable with non-luminescent authigenic quartz	oscillatory growth zoning
CL-SEM emission bands	650 nm	430 and 650 nm	500 and 650 nm	430 and 650 nm	variable	450 and 650 nm
Presence of fractures	thin, healed, brightly luminescent with mostly preferred orientation	randomly oriented, healed with non-luminescent quartz	not applicable	not applicable	not applicable	not applicable
Trace elements	abundant Al, Fe, K	abundant Al, Ti, Li	low Ti, Li	abundant Al, Ti, K	abundant Al, Ti, K	high Al, Ge
Al/Ti	1.6 to 375.1	1.6 to 11.6	56.2 to 119.6	3.7 to 5.9	3.15	425.4
Mineral micro inclusions	low variety	high variety	medium variety	medium variety	medium–high variety	
Lithological origin	metamorphic	undeformed plutonic	strongly altered plutonic	recrystallised (deformed) plutonic	sandstone-derived	hydrothermal
Provenance	Sierra Morena (Iberian Massif) and Sierra Nevada (Betic Cordilleras)	Los Pedroches batholith and associated plutons (Iberian Massif)	Los Pedroches batholith and associated plutons (Iberian Massif)	Los Pedroches batholith and associated plutons (Iberian Massif)	outcrops of Mesozoic and Cenozoic sandstones (Betic Cordilleras)	hydrothermal veins associated to Los Pedroches batholith and associated plutons (Iberian Massif)

luminescent micro-fractures, whereas these fractures are rare or absent in the Holocene ones (P4, P5 and PM), which suggests type 1 grains originate presumably from two metamorphic sequences. This is supported by there being two large massifs of metamorphic rocks of different ages and metamorphic history in the catchment area: the Sierra Morena mountains (Variscan orogeny; peak metamorphic age ~380 Ma) to the north and the Sierra Nevada mountains (Alpine orogeny; peak metamorphic age 30–15 Ma) to the south. During the long-lasting and much older Variscan orogeny, quartz of the metamorphic rock was exposed to multiple events of deformation and fracturing compared to quartz in rocks formed during the younger Alpine orogeny. Based on the different geological histories, type 1 quartz grains with healed fractures most likely originate from Variscan rocks, whereas the more homogenous (in SEM-CL) type 1 grains are from Alpine rocks.

The pre-Holocene samples (P1 and P2) contain more type 1 grains with healed fractures (Variscan protoliths) than Holocene samples (P4, P5 and PM). In turn, Holocene samples have more homogenous type 1 grains (Alpine protoliths). This change of the subgroups abundance could be related to the increase of the catchment area between 500 and 240 ka ago (Demuro et al., 2015; García-Tortosa et al., 2019) when Guadiana Menor (a side stream of Guadalquivir River) drained the endorheic lake in the Guadix-Baza basin. According to the presence of these subgroups, this event that took place after P2 (300 ka) was formed, extended the catchment area to Sierra Nevada (Alpine orogeny) and, for the first time, material from there could be transported and deposited in P3, P4 and P5 formations and PM.

The sedimentary type 5 quartz, rare and not present in all samples, most likely originates from the numerous outcrops of Mesozoic and Cenozoic sandstones scattered in the catchment area (Fig. 1b). It is, in fact surprising, that so few type 5 grains are preserved in the soils since sandstones are very common rocks in the centre of the catchment area. The primary origin of quartz grains constituting the eroded sandstones are both plutonic and metamorphic rocks.

The very distinctive type 6 grains originate from hydrothermal mineralisation. Abundant hydrothermal veins are associated with subvolcanic rocks of the Los Pedroches batholith and associated plutons. According to the classification of hydrothermal quartz by Rusk (2012) based on Ti and Al contents, type 6 quartz has Al and Ti values corresponding to epithermal and orogenic Au quartz.

There are differences in quartz grain populations among pre-Holocene samples (P1, P2 and P3): 1) P1 contains mostly metamorphic (type 1) and plutonic quartz of the strongly altered type (type 3); 2) in P2 mostly plutonic quartz (type 2) and 75% (15 out of 20 described) of the sandstone-derived quartz (type 5) were found; and 3) in P3 only plutonic quartz almost exclusively of the unaltered type (type 2) occurs. These differences could point to successive changes in the source area (P1 to P2, P2 to P3). The quartz population changes from P1 to P2 and P2 to P3 could be due to the increase of the catchment area, that took place between 500 and 240 ka (Demuro et al., 2015; García-Tortosa et al., 2019). Moreover, grains of easily erodible sandstone likely ended up in the soil during the initial stages of the extended catchment area. Later on, when the river had cut into the sandstone, quartz grains transported from further distances were deposited in the soils.

In contrast, the Holocene samples (P4, P5 and PM) are relatively similar in the abundance of quartz types. In all Holocene soils, undeformed plutonic quartz dominates (type 2). The source area appears stable throughout Holocene but is different from pre-Holocene times (change from P3 to P4).

5.2. Implications of mineral micro inclusions in quartz

Mineral micro inclusion species detected with SEM-EDX in quartz grains are typical minerals (Tables 3 and 5), described as rock-forming minerals in lithologies of the catchment area (Azcárate et al., 1977; Larrea et al., 2013). Thus, the micro inclusions identified in quartz can

be used as an additional indicator of grain provenance. Most of the identified minerals (feldspar, mica, zircon, iron oxides, monazite, rutile, ilmenite, apatite, barite) were described as the fine sand fraction constituents of these same soil samples (Martín-García et al., 2020).

Considering the mineralogical variety of micro inclusions by quartz type (Table 5), type 2 (undeformed plutonic quartz) has the greatest diversity, followed by type 5 (sandstone-derived quartz). It is not only the diversity but also the type of inclusions that are similar. The similarity between type 2 and type 5 grains could be because the grain cluster forming the sandstone fragments consists predominantly of plutonic quartz (type 2). It is noteworthy that Holocene type 2 samples (P4, P5 and PM) have more micro inclusions than pre-Holocene ones (P2 and P3), which is another indication of the change of the source area.

The identified feldspar micro inclusions (found in 36% of the grains) were K-feldspar or albite. Anorthite, Ca-bearing feldspar, was not found. This indicates that the plutonic source rocks represent fractionated granitic rocks, which crystallised K-feldspar and Ca-free or -poor plagioclase (albite). Mica micro inclusions (found in 27% of the grains) are generally smaller (mean 29 μm) in P1 quartz compared to other samples (103–205 μm). Although the mica inclusion size has high standard deviation values (Table 3), this difference in mica inclusion size could indicate different protoliths and, thus, changes in the catchment area between the deposition of the P1 and P2 terraces, as outlined above.

5.3. Trace element contents in the quartz types

Another approach to reveal the provenance of quartz grains and their change over time is comparing the trace element content of quartz grains in soils of different ages with quartz trace element contents of rocks in the catchment area (Table 4). However, no quartz trace element data are available for rocks exposed in the catchment area. Gárate-Olave et al. (2017) performed the closest quartz trace element study on igneous rocks of the Variscan Nisa-Alburquerque batholith about 315 km northwest of the study zone. However, the general trace element signature of quartz formed in different geological environments are well-known and, thus, can be used to determine the general protolith formation setting of quartz grains (e.g. Schrön et al., 1988; Götze et al., 2004; Jacamon and Larsen, 2009; Müller and Koch-Müller, 2009; Rusk, 2012).

The low Al, Ti and Li contents in grains of type 1 confirm the metamorphic formation conditions of this grain population (e.g. Müller et al., 2007; Müller and Koch-Müller, 2009). The detected trace elements contents are similar, for example, to those of sand quartz grains from soils of Sierra Nevada (Martín-García et al., 2004, 2015). The grains found in the Sierra Nevada soils were interpreted as weathering products of the underlying metamorphic rocks. The similarities in the trace element contents again support our statement that type 1 grains are derived from metamorphic rocks. The Al/Ti ratio of type 1 grains is higher in P1 samples (range 77–376) compared to grains in samples P2, P4 and P5 (<26). Although there are few analyses, the low Al/Ti values of grains from P2, P4 and P5 are similar to those of the Sierra Nevada quartz described by Martín-García et al. (2015) (23 ± 35). Low Al/Ti ratios indicate high formation temperatures (as discussed below) and, thus, the grains in P1 and the Sierra Nevada originate from low- to medium-grade metamorphic rocks and grains in P2, P4 and P5 from high-grade metamorphic rocks. This, in turn, could point to a significant change in the catchment area between 600 ka (P1) and the other terraces (P2, P3, P4, P5 and PM). There are other differences between pre-Holocene and Holocene samples in type 1. In pre-Holocene samples, there are higher contents of Al and B (in most cases). In addition, Na is always below the detection limit (<46.6 ppm), and Ca usually as well (<21.6 ppm) (Table SM1). In Holocene samples, however, concentrations of Na (frequently) and Ca (always) were above detection limits.

Concentrations of trace elements in type 2 grains are more homogeneous than type 1. However, differences between pre-Holocene and Holocene samples are observed for Na, Ca, Zn and Ga contents. Similar to type 1 grains, concentrations of Na in pre-Holocene samples are below the detection limit (<46.6 ppm) and that of Ca (<21.6 ppm) for the majority of results as well (Table 4). Trace element signature in type 2 agree with that of the quartz from Variscan granitic rocks in general (e.g. Müller et al.,2000, 2010; Breiter and Müller, 2009; Breiter et al.,2012, 2013, 2020). As mentioned above, Gárate-Olave et al. (2017) performed quartz trace element analyses on granitic rocks of the Variscan Nisa-Alburquerque batholith, the closest quartz chemistry study to our area. For comparison, our data of the igneous type 2 and type 3 grains were plotted with the data from the Nisa-Alburquerque batholith in the binary Al/Ti versus Ge/Ti plot (Fig. 5). The chemistries of our type 2 and 3 grains are within the range of the Variscan samples studied by Gárate-Olave et al. (2017).

According to Müller et al. (2002), Jacamon and Larsen (2009), and Breiter et al. (2013), increasing Al/Ti and Ge/Ti ratios in quartz indicate an increasing degree of fractionation of granitic magmas. Type 3 grains have significantly higher Al/Ti and Ge/Ti ratios than type 2 grains, indicating that the protolith of type 3 grains is a highly fractionated granite. The grains may even originate from pegmatite since ratios are in the range of the aplite-pegmatites of the Nisa-Alburquerque batholith (Gárate-Olave et al., 2017). That would also explain the strong alteration of type 3 grains: highly fractionated granites and pegmatites are enriched in volatiles, which react with and overprint already crystallised minerals during the late stage of melt crystallisation. The relative low Al/Ti and Ge/Ti ratios of type 3 grains indicate relative primitive granite compositions comparable to the monzogranites of the Nisa-Alburquerque batholith (Gárate-Olave et al., 2017).

The composite type 5 sandstone fragments contain plutonic and metamorphic quartz grains cemented by authigenic quartz. The Al/Ti ratio of the one analysed crystal is exceptionally low (~3), which suggest that the grain comes originally (before sandstone formation) from a chemical primitive pluton of the Iberian Massif pluton or high-grade metamorphic rocks of the Internal Betic Zones.

Based on the identified trace element correlations of type 1 grains in pre-Holocene (P1, P2, P3) and Holocene (P4, P5 and PM) samples, differences in trace element incorporation are observed (Figure SM1): the combined substitution of $Al^{3+} + K^+$ for Si^{4+} seems to be the prevailing process in pre-Holocene grains ($R^2 = 0.535$; n = 6) whereas the $Al^{3+} + Li^+$ substitution for Si^{4+} is the dominant one for the Al^{3+} defect charge compensation in Holocene grains ($R^2 = 0.967$, n = 4). This conclusion bases on the observed correlation between Al and K, and Al and Li, respectively.

Fig. 6 shows the compositional differences between the different grain types and confirms their genetic attributions. In the ternary Ti − 10*Ge - Al/50 plot, according to Schrön et al. (1988), type 2 grains (undeformed plutonic quartz) show a relative homogenous composition dominated by the Ti content. According to the Ti − 10*Ge - Al/50 discrimination, the type 2 grains originate from granites of primitive chemical (little fractionated) composition. The Al-Ge-Ti chemistries of
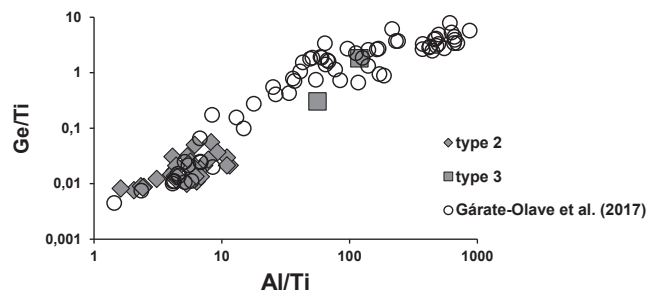

Fig. 5. Binary Al/Ti versus Ge/Ti plot showing the chemical variation of the type 2 and type 3 quartz grains from soil samples compared to quartz chemistries of the Variscan Nisa-Alburquerque batholith (open circles).
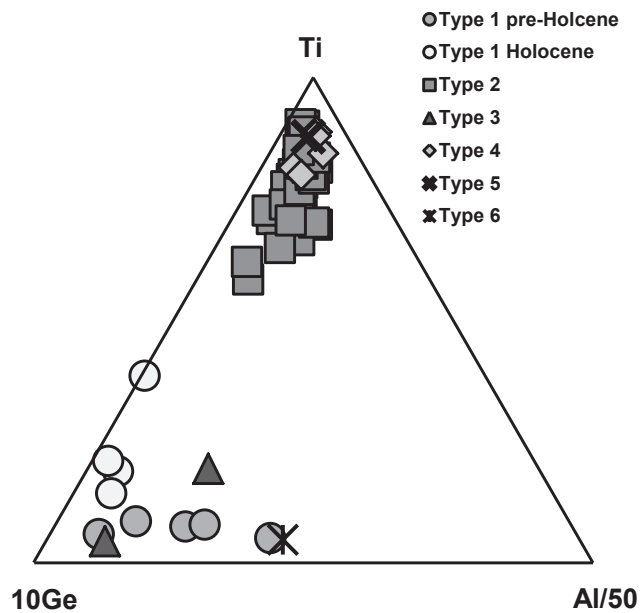
Fig. 6. Ternary Ti − 10*Ge - Al/50 plot according to Schrön et al. (1988) for trace elements in quartz showing the chemical variation of type 1 to 6 grains from sand fraction of soils.

type 4 (recrystallised plutonic quartz) and 5 (sandstone quartz) grains are in the same range as type 2 grains, which confirms, first, that type 4 grains were of plutonic origin before deformation and, second, that the one analysed type 5 grain from the sandstone fragment is also of plutonic origin. Type 1 (metamorphic quartz), 3 (strongly altered plutonic quartz) and 6 (hydrothermal quartz) grains plot close to the 10*Ge corner, indicating either that the grains originate from highly fractionated granitic rocks or hydrothermal mineralisation (e.g. Müller et al., 2018; Breiter et al., 2020).

5.4. Ti content in quartz as a geothermobarometer

Huang and Audétat (2012) modified the original Ti-in-quartz geothermometer by Wark and Watson (2006) to the TitaniQ geothermobarometer. The adjustment was based on the observation that the incorporation of Ti in the quartz lattice is controlled by temperature and, to a minor extent, by pressure. Thus, to calculate quartz crystallisation temperature, the approximate formation pressure and the Ti saturation of the fluid or melt from which the quartz crystallised must be known. In the catchment area, rock pressure and temperature conditions are highly variable. The metamorphic rocks of the Variscan Iberian Massif underwent multiple regional metamorphisms ranging from low (<2 kbar and 190–360 °C; Aparicio et al., 1997) to medium grades (green schist facies, 3.5–4 kbar and 350–400 °C; Larrea et al., 2013). Contact metamorphism occurred in the vicinity of the Los Pedroches batholith and its associated plutons (Linares and Santa Elena) with recorded pressures of <3 kbar and temperatures of 700 °C (Larrea, 1998). However, compared to the regional metamorphic rocks, the contact metamorphic rocks are exposed in small areas only. Igneous rocks of the Variscan Los Pedroches batholith were generated at 3 kbar and <750 °C, and associated subvolcanic rocks formed at <3 kbar and <750 °C (Larrea, 1998; Larrea et al., 2013). Metamorphic rocks of the Internal Zone of the Betic Cordilleras underwent medium-grade regional metamorphism with pressures of 3–9 kbar and temperatures of 430–540 °C for the Veleta Unit and 3.5–10 kbar and 480–630 °C for the Mulhacen Unit (Puga et al., 2007).

Subsequently, the known approximate pressures were applied to calculate the minimum crystallisation temperature of the analysed quartz grains using the equation of Huang and Audétat (2012). The resulting values are minimum crystallisation temperatures because the Ti saturation of the quartz-forming melts and fluids are unknown.

Type 1 quartz grains originate from metamorphic rocks either from the Iberian Massif with formation pressures between 3.5 and 4 kbar or from the Betic Cordilleras with pressure from 3 to 10 kbar. As suggested above, type 1 quartz in sample P1 is from the Iberian Massif while those from P2, P4 and P5 samples from both the Iberian Massif and Betic Cordilleras. This statement is supported by the findings of Demuro et al. (2015) and García-Tortosa et al. (2019), who suggested that the Internal Betic Zone that became the sediment source area about 500–240 ka ago caused a change in the grain population of samples P2, P4 and P5. The calculated formation temperatures of the type 1 grains in P1 are generally lower (404–454 °C) than those of type 1 grains in P2, P4 and P5 (452 - 791 °C) (Fig. 7). The calculated formation temperatures of all type 1 quartz are higher than the temperatures of the regional metamorphism of the Variscan rocks but agree with the metamorphic temperatures of the Betic Cordilleras rocks (Internal Zone; Puga et al., 2007). It is unlikely that the high-temperature type 1 quartz originated from Variscan contact metamorphic because these rocks occur in small outcrops only. The high crystallisation temperature of type 1 grain of sample P2 (791 °C) suggests this particular grain originates from a plutonic rock and not from metamorphic rock, as the SEM-CL observations imply.

Crystallisation temperatures of type 2 grains (plutonic quartz) are between 585 and 761 °C, which is, in general, the crystallisation range of granitic magmas. Larrea et al. (2013) stated that the crystallisation temperature of the Los Pedroches batholith was in the range of 700 to 750 °C. These temperatures are consistent with our type 2 crystallisation temperatures considering that the calculated values are minimum temperatures.

Temperatures calculated for type 3 grains (strongly altered plutonic quartz) are 384 to 494 °C. The low temperatures imply that the quartz alteration, presumably hydrothermal alteration, caused a release of Ti from the quartz lattice. Lillo-Ramos (1992), for example, described widespread hydrothermal alteration affecting the granodiorites of the Santa Elena pluton (Los Pedroches batholith).

Type 4 grains (recrystallised plutonic quartz) have crystallisation temperatures between 668 and 748 °C, which is in the range of the solidus temperature of granitic rocks. Thus, the deformation did not affect the quartz's Ti content, implying that type 4 quartz was exposed to low-temperature shear stress rather than regional medium- or high-grade metamorphism.

The plutonic crystal of the type 5 sandstone fragment had a crystallisation temperature of 705 °C (assuming about 3 kbar for magma crystallisation), confirming the igneous nature of the grain.

The hydrothermal type 6 quartz was formed at 431 °C, which is compatible with formation temperatures of granite-related magmatic-hydrothermal mineralisation commonly found in the Variscan plutons of the southern Iberian Massif (e.g. Chicharro et al., 2016).

5.5. Quartz in soil chronosequence

In a soil chronosequence, which is defined as a series of genetically related soils that evolve under similar conditions of vegetation, parent rock, topography and climate (Harden, 1982), both soil properties and constituents can be statistically related to the soil age, and thus constitute chronofunctions. The samples used in this study belong to a genuine soils chronosequence where chronofunctions have been established using morphological, analytical and compositional properties (Calero et al., 2008, 2009, 2013; Martín-García et al., 2016, 2020).

However, using the sand fraction (500–2000 μm) of the same soils in this study, no chronofunctions have been detected for the quartz trace elements compositions or the quartz type abundance, except for the abundance of type 4 per profile ($R^2 = 0.864$). Nevertheless, differences are observed in pre-Holocene and Holocene samples, mainly due to changes in the source area rather than soil-forming processes.
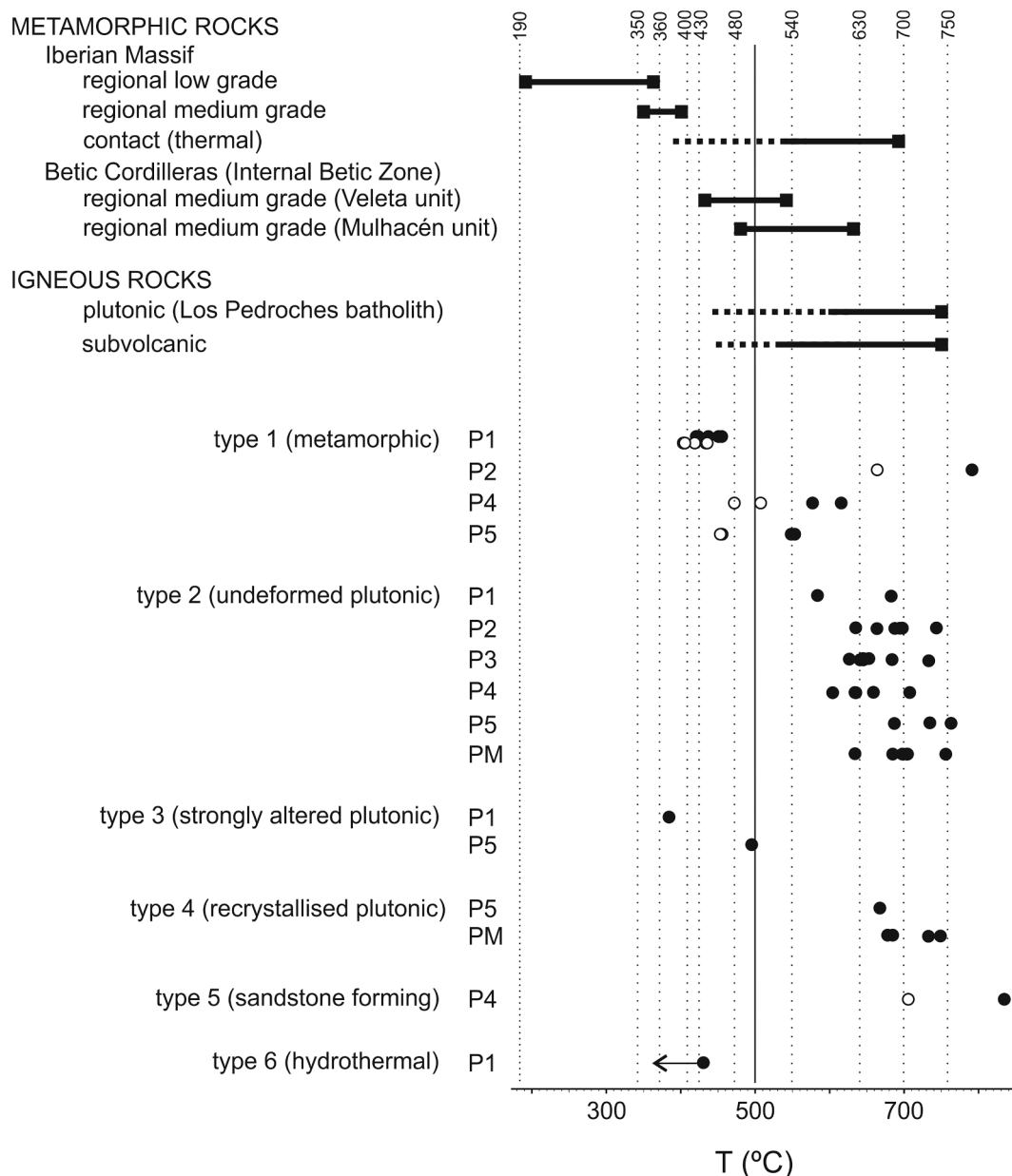
Fig. 7. Calculated minimum crystallization temperatures of analysed quartz grains in soil samples according to the TitaniQ thermobarometer for quartz. For comparison, literature data of formation temperatures of metamorphic and igneous rocks of the Variscan Iberian Massif and the Alpine Betic Cordilleras located in the catchment area of the Guadalquivir River are provided. Open circles are values applying the minimum pressure scenario and black circles the maximum pressure scenario.

Martín-García et al. (2015) found in the fine sand of soil from Sierra Nevada (Guadalquivir catchment) a relative enrichment in trace elements by comparing the edges of grains with their centres attributed to the pedological evolution. These authors demonstrated an increase in the content of trace elements on the edge of the quartz grain following the evolutionary sequence of the soil: parent rock < Entisol < Inceptisol < Alfisol; this was corroborated by the SEM study of the surface of these grains (W of Marcelino et al., 1999) in which signs of alteration increased with the evolution of the soil. However, the absence of these differences in this study could be due to: 1) different fractions were used to carry out the study: fine sand (Martín-García et al., 2004, 2015) *vs* coarse sand (this study); 2) fine sand is a granulometric fraction more weathered than coarse sand (similar to parent rock); 3) different methods of study and equipment were used: in the fine sand studied by Martín-García et al. (2004, 2015), the centre and edge of quartz grains were analysed with EMPA with an analytical spot of about 10 μm, while

in this study, only the centres of quartz grains were analysed by LA-ICP-MS, applying a raster ablation of about 150x100 μm. However, the SEM-CL research of our study shows that there are no differences in CL between the core and the crystal rim, suggesting that the trace element contents are more or less consistent across the grain (e.g. Götze et al., 2001).

Concluding, the compositional changes of the surface of fine sand-sized quartz grains observed by Martín-García et al. (2004, 2015) is related to surface alteration processes related to the soil formation, while the analysis of the composition of the interior of coarse sand quartz grains (this study) and SEM-CL analysis, allows obtaining information about the lithological origin and infer their source area.

6. Conclusions

Based on SEM-CL characteristics, micro inclusion inventory and

trace element contents of quartz grains from soil sand fraction of Guadalquivir River terraces, six types of grains have been distinguished: metamorphic quartz (type 1), undeformed granitic quartz (type 2), strongly altered granitic quartz (type 3), recrystallised (deformed) granitic quartz (type 4), sandstone quartz (type 5) and hydrothermal quartz (type 6).

The major quartz grain types (76% of the grains) are undeformed granitic quartz (type 2) and metamorphic quartz (type 1). All quartz grains of granitic origin (types 2, 3 and 4) are interpreted to come from the Los Pedroches batholith and its associated plutons (Santa Elena and Linares plutons). Metamorphic quartz grains (type 1) have two possible sources: Sierra Morena (Iberian Massif) to the north or Sierra Nevada (Betic Cordilleras) to the south. The metamorphic quartz grains of terrace P1 originate exclusively from the Iberian Massif. Grains of the younger P4 and P5 terraces come from both source areas. However, the origin of P2 grains is dubious due to the uncertainty about when the extension of the catchment area took place. The sandstone-derived quartz grains (type 5) most likely originate from the numerous outcrops of Mesozoic and Cenozoic sandstones scattered in the central catchment area. The sandstone-derived grains comprise quartz crystals, the primary origin of those are both granitic and metamorphic rocks. Hydrothermal quartz grains (type 6) come from hydrothermal quartz veins associated with subvolcanic rocks of the Los Pedroches batholith.

The quartz type contents in pre-Holocene soils (P1, P2 and P3) are more variable than in Holocene soils (P4 and P5), which are more homogeneous. This difference could be attributed to changes in the source area over time, which affected the materials that form the soils.

Our study shows that the characterisation of quartz grains by applying SEM-CL, SEM-EDX and LA-ICP-MS is an effective methodological approach to characterise the provenance of quartz grains in the sand fraction of soils and substantially improves the knowledge of the sedimentological history of the Guadalquivir River terraces.

Declaration of Competing Interest

The authors declare that they have no known competing financial interests or personal relationships that could have appeared to influence the work reported in this paper.

Acknowledgements

Appendix A. Supplementary data

Supplementary data to this article can be found online at https://doi.org/10.1016/j.geoderma.2022.115769.

References

Ackerson, M.R., Tailby, N.D., Watson, E.B., 2015. Trace elements in quartz shed light on sediment provenance. Geochem. Geophys. Geosyst. 16 (6), 1894–1904.

Aparicio, A., García, R., Brell, J.M., 1997. El metamorfismo de bajo y muy bajo grado de los materiales carboníferos del área hercinica de Sierra Morena. Boletín geológico y minero 108 (2), 171–184.

Azcárate, J.E., Esnaola, J.M., Maldonado, M., del Pan T., Perconig, E., Moreno, E., Argüelles, A., Martínez, J.U., Fernández, Luanco, M.C., Solar, J.B., 1977. Mapa geológico y memoria de la hoja n° 905 (Linares). Mapa Geológico de España E. 1: 50.000 (MAGNA). Segunda Serie, Primera edición. IGME. Depósito Legal: M-18.924 -1977.

Bambauer, H.U., 1961. Spurenelementgehalte und γ-Farbzentren in Quarzen aus Zerrklüften der Schweizer Alpen. Schweizerische Mineralogische und Petrographische Mitteilungen 41, 335–369.

Bernet, M., Bassett, K., 2005. Provenance analysis by single-quartz-grain SEM-CL/optical microscopy. J. Sediment. Res. 75 (3), 492–500.

Blatt, H., Middleton, G.V., Murray, R.C., 1980. Origin of Sedimentary Rocks. Prentice-Hall Inc, Englewood Cliffs, NJ.

Breiter, K., Müller, A., 2009. Evolution of rare-metal granitic magmas documented by quartz chemistry. Eur. J. Mineral. 21, 335–346.

Breiter, K., Svojtka, M., Ackerman, L., Švecová, K., 2012. Trace element composition of quartz from the Variscan Teplice caldera (Krušné Hory/Erzgebirge Mts., Czech Republic/Germany): insights into the volcano-plutonic complex evolution. Chemical Geology 326–327, 36–50.

Breiter, K., Ackerman, L., Svojtka, M., Müller, A., 2013. Behavior of trace elements in quartz from plutons of different geochemical signature: A case study from the Bohemian Massif, Czech Republic. Lithos 175-176, 54–67.

Breiter, K., Ďurišová, J., Dosbaba, M., 2020. Chemical signature of quartz from S- and A-type rare-metal granites – A summary. Ore Geol. Rev. 125, 103674. https://doi.org/10.1016/j.oregeorev.2020.103674.

Calero, J., Delgado, R., Delgado, G., Martín-García, J.M., 2008. Transformation of categorical field soil morphological properties into numerical properties for the study of chronosequences. Geoderma 145 (3-4), 278–287.

Calero, J., Delgado, R., Delgado, G., Martín-García, J.M., 2009. SEM image analysis in the study of a soil chronosequence on fluvial terraces of the middle Guadalquivir (southern Spain). Eur. J. Soil Sci. 60 (3), 465–480.

Calero, J., Martín-García, J.M., Delgado, G., Aranda, V., Delgado, R., 2013. A nano-scale study in a soil chronosequence from southern Spain. Eur. J. Soil Sci. 64 (2), 192–209.

Chicharro, E., Boiron, M.-C., López-García, J.Á., Barfod, D.N., Villaseca, C., 2016. Origin, ore forming fluid evolution and timing of the Logrosán Sn–(W) ore deposits (Central Iberian Zone, Spain). Ore Geol. Rev. 72, 896–913.

Demuro, M., Arnold, L.J., Parés, J.M., Sala, R., 2015. Extended-range luminescence chronologies suggest potentially complex bone accumulation histories at the Early-to-Middle Pleistocene palaeontological site of Huéscar-1 (Guadix-Baza basin, Spain). Quat. Int. 389, 191–212.

Drees, L.R., Wilding, L.P., Smeck, N.E., Senkayi, A.L., 1989. Silica in soils: quartz and disordered silica polymorphs. In: Dixon, J.B., Weed, S.B. (Eds.), Minerals in Soil Environments. Soil Science Society of America, Madison, WI, pp. 913–965.

Gárate-Olave, I., Müller, A., Roda-Robles, E., Gil-Crespo, P.P., Pesquera, A., 2017. Extreme fractionation in a granite–pegmatite system documented by quartz chemistry: The case study of Tres Arroyos (Central Iberian Zone, Spain). Lithos 286-287, 162–174.

García-Tortosa, F.J., García, P.A., Giralt, S., Medina, I., Herrera, A.A., Rojas, I.M., 2019. Edad de la captura de la cuenca de Guadix-Baza. In XV Reunión Nacional de Cuaternario Bizkaia Aretoa-Bilbao. Universidad del País Vasco/Euskal Herriko Unibertsitatea, pp. 273–276, 1–5 julio 2019 libro de resúmenes.

Götze, J., 2009. Chemistry, textures and physical properties of quartz – geological interpretation and technical application. Mineral. Mag. 73 (4), 645–671.

Götze, J., 2012. Mineralogy, geochemistry and cathodoluminescence of authigenic quartz from different sedimentary rocks. In: Götze, J., Möckel, R. (Eds.), Quartz: Deposits, Mineralogy and Analytics. Springer, Berlin, Heidelberg, pp. 287–306.

Götze, J., Plötze, M., Habermann, D., 2001. Origin, spectral characteristics and practical applications of the cathodoluminescence (CL) of quartz–a review. Mineral. Petrol. 71 (3-4), 225–250.

Götze, J., Plötze, M., Graupner, T., Hallbauer, D.K., Bray, C.J., 2004. Trace element incorporation into quartz: a combined study by ICP-MS, electron spin resonance, cathodoluminescence, capillary ion analysis, and gas chromatography. Geochim. Cosmochim. Acta 68 (18), 3741–3759.

Harden, J.W., 1982. A quantitative index of soil development from field descriptions: examples for a chronosecuence in central California. Geoderma 28, 1–28.

Huang, R., Audétat, A., 2012. The titanium-in-quartz (TitaniQ) thermobarometer: a critical examination and re-calibration. Geochim. Cosmochim. Acta 84, 75–89.

IUSS Working Group WRB. 2015. World Reference Base for Soil Resources 2014, update 2015 International soil classification system for naming soils and creating legends for soil maps. World Soil Resources Reports No. 106. FAO, Rome.

Jacamon, F., Larsen, R.B., 2009. Trace element evolution of quartz in the charnockitic Kleivan granite, SW-Norway: the Ge/Ti ratio of quartz as an index of igneous differentiation. Lithos 107 (3-4), 281–291.

Jochum, K.P., Weis, U., Stoll, B., Kuzmin, D., Yang, Q., Raczek, I., Jacob, D.E., Stracke, A., Birbaum, K., Frick, D.A., Günther, D., Enzweiler, J., 2011. Determination of reference values for NIST SRM 610–617 glasses following ISO guidelines: Geostand. Geoanalyt. Res. 35 (4), 397–429.

Kats, A., 1962. Hydrogen in alpha quartz. Philips Research Reports 17, 133–279.

Larrea, F.J., 1998. Caracterización petrológica y geoquímica del sector oriental del batolito de Los Pedroches. Universidad del Pais Vasco, Tesis Doctoral.

Larrea, F.J., Santisteban, J.I., Cueto, L.A., Quesada, C., Fernández, F.J., Martín-Serrano, Á., La Moneda, E., Bea Barredo, F., González, A., Matas, J., Martín, L.M., Vallejo, J., López, M.A., 2013. Mapa geológico y memoria de la hoja n° 904 (Andújar). Mapa Geológico de España E. 1:50.000 (MAGNA). Segunda Serie, Primera edición. IGME. Depósito legal: M–34940–2013.

Larsen, R.B., Polvè, M., Juve, G., 2000. Granite pegmatite quartz from Evje-Iveland: Trace element chemistry and implications for the formation of high-purity quartz: Norges Geologiske Undersøkelse. Bulletin 436, 57–65.

Lillo-Ramos, F.J., 1992. Geology and geochemistry of Linares-La Carolina Pb-ore field (Southeastern border of the Hesperian Massif). University of Leeds. Doctoral dissertation.

Mahaney, W.C., 2002. Atlas of Sand Grain Surface Textures and Applications. Oxford University Press, Oxford, UK.

Marcelino, V., Mussche, G., Stoops, G., 1999. Surface morphology of quartz grains from tropical soils and its significance for assessing soil weathering. Eur. J. Soil Sci. 50, 1–8.

Martín-García, J.M., Aranda, V., Gámiz, E., Bech, J., Delgado, R., 2004. Are mediterranean mountains entisols weakly developed? The case of orthents from Sierra Nevada (southern Spain). Geoderma 118 (1–2), 115–131.

Martín-García, J.M., Márquez, R., Delgado, G., Sánchez-Marañón, M., Delgado, R., 2015. Relationships between quartz weathering and soil type (Entisol, Inceptisol and Alfisol) in Sierra Nevada (southeast Spain). Eur. J. Soil Sci. 66 (1), 179–193.

Martín-García, J.M., Molinero-García, A., Calero, J., Sánchez-Marañón, M., Fernández-González, M.V., Delgado, R., 2020. Pedogenic information from fine sand: A study in Mediterranean soils. Eur. J. Soil Sci. 71 (4), 580–597.

Martín-García, J.M., Sánchez-Marañón, M., Calero, J., Aranda, V., Delgado, G., Delgado, R., 2016. Iron oxides and rare earth elements in the clay fractions of a soil chronosequence in southern Spain. Eur. J. Soil Sci. 67 (6), 749–762.

McDonough, W.F., Sun, S.-s., 1995. The composition of the Earth. Chemical Geology 120 (3-4), 223–253.

Müller, A., 2000. Cathodoluminescence and characterisation of defect structures in quartz with applications to the study of granitic rocks. Niedersächsische Staats-und Universitätsbibliothek Göttingen). Doctoral dissertation.

Müller, A., Seltmann, R., Behr, H.J., 2000. Application of cathodoluminescence to magmatic quartz in a tin granite – case study from the Schellerhau Granite Complex. Miner. Depos. 35, 169–189.

Mü ller, A., Wiedenbeck, M., van den Kerkhof, A.M., Kronz, A., Simon, K., 2003. Trace elements in quartz – a combined electron microprobe, secondary ion mass spectrometry, laser-ablation ICP-MS, and cathodoluminescence study. Eur. J. Mineral. 15 (4), 747–763.

Müller, A., Ihlen, P.M., Wanvik, J.E., Flem, B., 2007. High-purity quartz mineralisation in kyanite quartzites. Norway. Miner. Depos. 42 (5), 523–535.

Müller, A., Koch-Müller, M., 2009. Hydrogen speciation and trace element contents of igneous, hydrothermal and metamorphic quartz from Norway. Mineral. Mag. 73 (4), 569–583.

Müller, A., Wiedenbeck, M., Flem, B., Schiellerup, H., 2008. Refinement of phosphorus determination in quartz by LA-ICP-MS through defining new reference material values: Geostand. Geoanalyt. Res. 32 (3), 361–376.

Müller, A., Herrington, R., Armstrong, R., Seltmann, R., Kirwin, D.J., Stenina, N.G., Kronz, A., 2010. Trace elements and cathodoluminescence of quartz in stockwork veins of Mongolian porphyry-style deposits. Miner. Depos. 45 (7), 707–727.

Müller, A., Kronz, A., Breiter, K., 2002. Trace elements and growth patterns in quartz: a fingerprint of the evolution of the subvolcanic Podlesí Granite System (Krušné hory Mts., Czech Republic). Bull. Czech Geol. Surv. 77, 135–145.

Müller, A., Knies, J., 2013. Trace elements and cathodoluminescence of detrital quartz in Arctic marine sediments–a new ice-rafted debris provenance proxy. Clim. Past 9 (6), 2615–2630.

Müller, A., Herklotz, G., Giegling, H., 2018. Chemistry of quartz related to the Zinnwald/Cínovec Sn-W-Li greisen-type deposit, Eastern Erzgebirge. Germany. J. Geochem. Explor. 190, 357–373.

Ortiz, J.E., Torres, T., Llamas, J.F., Canoira, L., García-Alonso, P., García de la Morena, M.A., Lucini, M., 2000. Dataciones de algunos yacimientos paleontológicos de la cuenca de Guadix-Baza (sector de Cúllar-Baza, Granada, España) y primera estimación de edad de la apertura de la cuenca mediante el método de racemización de aminoácidos. Geogaceta 28, 109–112.

Perny, B., Eberhardt, P., Ramseyer, K., Mullis, J., Pankrath, R., 1992. Microdistribution of Al, Li, and Na in α quartz: Possible causes and correlation with short-lived cathodoluminescence. Am. Mineral. 77, 534–544.

Puga, E., de Federico, A.D., Nieto, J.M., Puga, M.D., 2007. Petrología, evolución geodinámica y georrecursos del Espacio Natural de Sierra Nevada. Estud. Geol. 63 (2), 19–40.

Ramseyer, K., Mullis, J., 1990. Factors influencing short-lived blue cathodoluminescence of alpha-quartz. Am. Mineral. 75 (7–8), 791–800.

Richter, D.K., Götte, T., Götze, J., Neuser, R.D., 2003. Progress in application of cathodoluminescence (CL) in sedimentary geology. Mineral. Petrol. 79, 127–166.

Rimstidt, J.D., 1997. Quartz solubility at low temperatures. Geochim. Cosmochim. Acta 61 (13), 2553–2558.

Rottier, B., Rezeau, H., Casanova, V., Kouzmanov, K., Moritz, R., Schlöglova, K., Wälle, M., Fontboté, L., 2017. Trace element diffusion and incorporation in quartz during heating experiments. Contrib. to Mineral. Petrol. 172 (4), 23.

Rusk, B.G., Lowers, H.A., Reed, M.H., 2008. Trace elements in hydrothermal quartz: Relationships to cathodoluminescent textures and insights into vein formation. Geology 36 (7), 547. https://doi.org/10.1130/G24580A.110.1130/2008132.

Rusk, B., 2012. Cathodoluminescent Textures and Trace Elements in Hydrothermal Quartz. In: Götze, J., Möckel, R. (Eds.), Quartz: Deposits, Mineralogy and Analytics. Springer Geology, Springer, Berlin, Heidelberg, pp. 307–329.

Sales de Oliveira, C.E., Pe-Piper, G., Piper, D.J.W., Zhang, Y., Corney, R., 2017. Integrated methodology for determining provenance of detrital quartz using optical petrographic microscope and cathodoluminescence (CL) properties. Mar. Pet. Geol. 88, 41–53.

Schrön, W., Schmädicke, E., Thomas, R., Schmidt, W., 1988. Geochemische Untersuchungen an Pegmatitquarzen. Zeitschrift für Geologische Wissenschaften 16, 229–244.

Stalder, R., Potrafke, A., Billström, K., Skogby, H., Meinhold, G., Gögele, C., Berberich, T., 2017. OH defects in quartz as monitor for igneous, metamorphic, and sedimentary processes. Am. Mineral. 102 (9), 1832–1842.

Wark, D.A., Watson, E.B., 2006. TitaniQ: a titanium-in-quartz geothermometer. Contrib. to Mineral. Petrol. 152 (6), 743–754.

Weil, J.A., 1984. A review of electron spin spectroscopy and its application to the study of paramagnetic defects in crystalline quartz. Phys. Chem. Miner. 10 (4), 149–165.

Weil, J.A., 1993. A review of the EPR spectroscopy of the point defects in α-quartz: the decade 1982–1992. In: Helms, C.R., Deal, B.E. (Eds.), Physics and Chemsitry of SiO2 and the Si-SiO interface 2. Plenum Press, New York, pp. 131–144.